VII International Conference on Computational Methods in Marine Engineering
MARINE 2017
M. Visonneau, P. Queutey and D. Le Touzé (Eds)

A VOLUME-PRESERVING INFLOW BOUNDARY BASED NUMERICAL TANK APPLIED TO WAVE-STRUCTURE INTERACTION IN NEAR-SHALLOW WATER

SHASWAT SAINCHER*† AND JYOTIRMAY BANERJEE†

†Department of Mechanical Engineering, Sardar Vallabhbhai National Institute of Technology
Surat 395007, Gujarat, India. Fax: +91 261 2228394
e-mail*: shaswat.saincher@gmail.com, web page†: `http://www.svnit.ac.in`

Key words: Volume-preserving, Navier-Stokes, numerical wave tank, steep waves, kinematic stretching, wave-structure interaction

Abstract. *Inflow-boundary based Navier-Stokes (NSE) wave tanks are prone to volume addition, especially whilst generating steep* ($H/\lambda > 0.03$) *waves in near-shallow water* ($kh < 1$). *In the present work, a volume-preserving, inflow boundary based numerical tank is proposed in the two-phase NSE framework. Volume effluxed under troughs is balanced against that influxed under crests using kinematic stretching. The wave tank is tested for generation of steep* ($H/\lambda = 0.037, 0.048$), *trochoidal waves in near-shallow water* ($kh \approx 0.8$). *A comparison with baseline inflow formulation demonstrates that the proposed inlet boundary effectively restricts volume addition without inducing wave distortion. The NWT model is later implemented to wave-structure interaction occurring during low frequency* ($T = 2\,s$) *wave propagation over a submerged trapezoidal bar. Good agreement with experimental data is reported.*

1 INTRODUCTION

Numerical wave tanks (NWTs) are the computational counterpart of wave flumes. Over the past three decades, NWTs have emerged as a much needed secondary standard (to wave flumes) for addressing a wide variety of challenging problems in marine and coastal engineering as well as in physical oceanography. A few important examples include vortex dynamics of breaking waves, performance evaluation of wave energy converters [1], motion response of ships in waves and wave-structure interaction [2]. In order to design numerical algorithms for addressing the above-mentioned problems, one requires prior knowledge of the degree of complexity involved in each case. This would in turn enable one to develop algorithms with an *optimum level of complexity* that ensures a sustainable utilization of computational resources. For instance, the kinematics of ocean wave propagation is (for the most part) irrotational which lends simplification to numerical modeling and even opens avenues for analytical treatment in some cases. An apt example for the latter would be the development and subsequent application of the quasi-determinism theory [3] towards simulation of freak waves, wave groups and interaction and diffraction of wave groups past obstacles in a semi-analytical framework. Naturally, many of the pioneering (and even some

recent) works in NWT modeling were based on a potential (inviscid) flow assumption using the Boussinesq or Laplace equations [2]. The potential flow approach has an obvious advantage in that the framework of equations governing wave motion has the free surface elevation η and velocity potential ϕ as *explicit variables* for which the system could be solved. In addition to this, the $\phi - \eta$ framework allows a (relatively) coarser spatio-temporal discretisation to be realized in the NWT ($\lambda/\Delta x \sim 30$ and $T/\Delta t \sim 40$) [2] without risking numerical damping of the generated waves. Inviscid NWT formulations have been successfully applied to problems such as non-linear wave propagation, wave transformation and generation and evolution of focused waves [2].

Despite it's advantages, the inviscid framework is insufficient for describing the hydrodynamics of waves if there is an occurrence of large velocities $\gg C$ (where C is wave celerity) and/or if there is significant interplay between air and water "phases". Apt examples for this include wave breaking, wave mechanics in steep sea-states, interaction of breaking waves with structures and hydrodynamics of oscillating water column (OWC) type wave energy converters [1]. In such scenarios, the effect of molecular (and/or turbulent) viscosity and/or the presence of the air phase on wave kinematics can no longer be neglected. This necessitates development of viscous NWT models [4, 5] based on the Navier-Stokes equations (NSE) that, in reality, govern ocean wave propagation and facilitate the highest fidelity description of a given problem.

In case of NSE formulations, η and ϕ no longer (explicitly) appear as variables and the same need to be implicitly linked to the framework of governing equations. In a viscous NWT, the free surface displacement η needs to be correlated to the topology of the air-water interface. This necessitates a two-phase description of the fluid domain which could be achieved using (say) the VOF method [6]. Further, the potential $\phi(t)$ (determined apriori from wave theory) can be used to impose local, Dirichlet prescriptions of $U(t), V(t)$ (and $\eta(t)$) at so-called "inflow-boundaries" [4] that act as wave-generating boundary conditions for the momentum equations. However, inclusion of ϕ in NSE-based wavemaker formulations is not mandatory as wave generation could simply be achieved by specifying a "mass-source", based on $\eta(t)$, in the continuity equation for few cells comprising a "source region" [5]. In contrast to inviscid wave tanks, there is added complication in viscous NWTs to minimise artificial damping imposed by various numerical approximations made in the flow solver [6]. The need for minimizing numerical damping imposes limits on the coarsest spatio-temporal resolution that is permissible for a given wave design. Experience with numerical wave generation by the authors [6] indicates that NSE-based NWTs demand very fine temporal resolution ($T/\Delta t \geq 3000$) when $H/\lambda \leq 0.01$ (especially if $kh < 1$) whilst a refined spatial resolution ($\lambda/\Delta x \geq 150$) becomes necessary when $H/\lambda > 0.03$. These numbers are in sharp contrast to those mentioned earlier for a $\phi - \eta$ based NWT model [2].

It is evident that two-phase Navier-Stokes based NWT simulations are challenging. It can be further stated that the task of viscous wave generation becomes especially difficult in near-shallow water ($kh < 1$). The difficulty manifests itself in two ways:

- the water column has poor $U-$momentum damping characteristics for $kh < 1$. Wave generation is hence prone to occurrence of wave-vorticity interactions that (might) induce height damping in near-field of the wavemaker [6] and
- Stokes drift induced by the waves increases as $(\sinh kh)^{-2}$. Therefore, NWT simulations in $kh < 1$ are prone to wave setup resulting from volume addition.

The problem of volume addition can be prevented using a source-function wavemaker which is designed based on free-surface elevation $\eta(t)$ of the target waveform [5]. Since $\int_T \eta(t)\,\mathrm{d}t = 0$ over a wave period T, source-function based NWTs have excellent volume conservation properties. However, when $kh < 1$, jets of volume ejected from the source region lead to pervasive vortex formation which induces wave distortion and viscous height damping in the near-field [6]. The issue of near-field height damping can be resolved using an inflow-boundary based generator which is designed based on $U, V, \eta(t)$ of the targeted waves. In this case, initial momentum lost to vorticity is minimal because volume is *influxed* (rather than *ejected*) into the domain through the inflow-boundary. However, (water) volume influx and efflux into the tank depends on $U(y,t)$ and $\int_T \int_{h+\eta(t)} U(y,t)\,\mathrm{d}y\,\mathrm{d}t \neq 0$ at any order (of `Stokes` theory). Hence, there is net volume addition through an inflow boundary which induces setup for longer simulations ($t > 10T$).

Apparently, the task of designing a NSE-based NWT for $kh < 1$ is faced with contrasting challenges that necessitate modifications in baseline wavemaker formulation; such a modification has already been proposed by the authors [6] in a source-function based wavemaker for $kh \approx 0.8$. However, if volume-preserving, an inflow-boundary based wavemaker should be preferred over a source-function technique because (a) there is an obvious reduction in the number of design variables and (b) the computational domain is only to be modeled at one end of the wavemaker. Hence, in the present work, we extend the capabilities of our existing NSE-based PLIC-VOF NWT model [6] by introducing a volume-preserving inflow boundary based wavemaker and a simplified methodology for treatment of immersed boundaries. The mathematical formulation of the tank is presented in section 2. Volume conservation properties of the baseline inflow boundary have been improved using the concept of kinematic stretching [9] which is discussed in section 2.3. Boundaries of immersed structures in the tank (if any) have been approximated using non-uniform, stair-stepped meshes employing a staggered variable arrangement; said implementations are presented in section 3. The proposed NWT model has been tested for generation of steep regular waves ($H/\lambda = 0.037, 0.048$) in near-shallow water and validated against the experiments of Beji and Battjes [10] involving sinusoidal low frequency (SL) wave transformation over a submerged trapezoidal bar. Results obtained from these benchmarking tests are discussed in section 4. Major conclusions are presented in section 5.

2 Numerical wave tank

In the present work, an existing PLIC-VOF based NWT model, developed previously by the authors [6] has been modified by replacing the mass-source based wavemaker with an inflow-boundary based formulation. In addition, a simplified methodology (involving stair-stepping of the mesh) is introduced for simulating interactions between waves and submerged structures. Mathematical model of the tank is detailed in the following subsections.

2.1 Governing equations

The numerical wave tank has been modeled in a two-phase NSE framework. Wave propagation is considered as a simultaneous flow of air and water using the VOF method. This is done by defining the volume fraction f as the fraction of the primary phase (water) within a

computational cell. The transport of f is governed by the unsteady advection equation (1),

$$\iiint_{C\forall} \frac{\partial f}{\partial t} d\forall + \iint_{CS} \left(\vec{V} f\right) \bullet d\vec{A} = 0 \tag{1}$$

where, $\vec{V}$ denotes the advecting velocity, t is time and $d\vec{A}$ is the area of the surface surrounding the control volume $d\forall$. Equation (1) is solved geometrically using Youngs PLIC-VOF algorithm which is based on the recurrence of two steps; interface reconstruction and interface advection. In the first stage, the air-water interface is reconstructed using the gradient of the volume fraction field. The advection of the reconstructed fluid region is operator-split and comprises of consecutive sweeps along the x and $y-$ directions. The sweeping direction is alternated every time step for second-order accuracy and a conservative volume redistribution algorithm is run after each sweep to eliminate overshoots ($f > 1$) and undershoots ($f < 0$) in the volume fraction field. Wave motion is governed by solution of the two-phase NSE,

$$\begin{aligned}
&\iint_{CS} \vec{V} \bullet d\vec{A} = 0 \\
&\iiint_{C\forall} \frac{\partial U}{\partial t} d\forall + \iint_{CS} \left(U\vec{V}\right) \bullet d\vec{A} = -\frac{1}{\rho^*} \iiint_{C\forall} \frac{\partial p}{\partial x} d\forall + \frac{1}{\rho^*} \iint_{CS} \left(\mu^* \vec{\nabla} U\right) \bullet d\vec{A} \\
&\iiint_{C\forall} \frac{\partial V}{\partial t} d\forall + \iint_{CS} \left(V\vec{V}\right) \bullet d\vec{A} = -\frac{1}{\rho^*} \iiint_{C\forall} \frac{\partial p}{\partial y} d\forall + \frac{1}{\rho^*} \iint_{CS} \left(\mu^* \vec{\nabla} V\right) \bullet d\vec{A} - \iiint_{C\forall} g d\forall
\end{aligned} \tag{2}$$

where, U and V denote the streamwise (x) and vertical (y) components of velocity, p is the pressure, ρ^* and μ^* are the mixture density and mixture viscosity respectively and g is the acceleration due to gravity. The mixture properties are calculated as,

$$\rho^* = f\rho_w + (1-f)\rho_a \;\; \text{and} \;\; \mu^* = f\mu_w + (1-f)\mu_a \tag{3}$$

where subscripts w and a denote the water and air phases respectively. As mentioned previously, there is an added task of minimising *numerical damping* of wave height in NSE-based NWTs [6]. It is difficult to eliminate all sources of numerical damping, however, as suggested by Perić and Abdel-Maksoud [7], the errors introduced by numerical approximations can be reduced (but not eliminated) by designing a sufficiently fine computational mesh. Hence, in NSE-based NWT formulations, more emphasis is laid upon mesh design (especially for steep waves) for arresting artificial damping [5, 6, 7]. NWT domain configuration and meshing strategy are presented in the next subsection.

2.2 Domain and mesh configuration

The computational model of the numerical wave tank is shown in figure 1. Two separate configurations of the tank (differing chiefly in the manner in which waves are damped) have been formulated for simulating regular trochoidal waves and transformation of SL waves. Model parameters have been represented here in a generalized manner; problem-specific values of design variables are reported in section 4. With reference to figure 1, $\mathbb{L}$ is the length of the wave

simulation region, $\mathbb{H}$ is the height of the domain, ℓ_d is the length of sponge layer and h is the still water depth. Variables characterizing the mesh structure are also shown; nx and ny represent the total number of cells along the x and y directions respectively, nxm is the number of cells in the wave simulation region, nxr denotes the number of cells in the east sponge layer (ESL) and nyu, nyd denote the number of vertical cells above and below the still water level (SWL) respectively. Two additional variables have been derived: number of cells per wavelength nx_λ

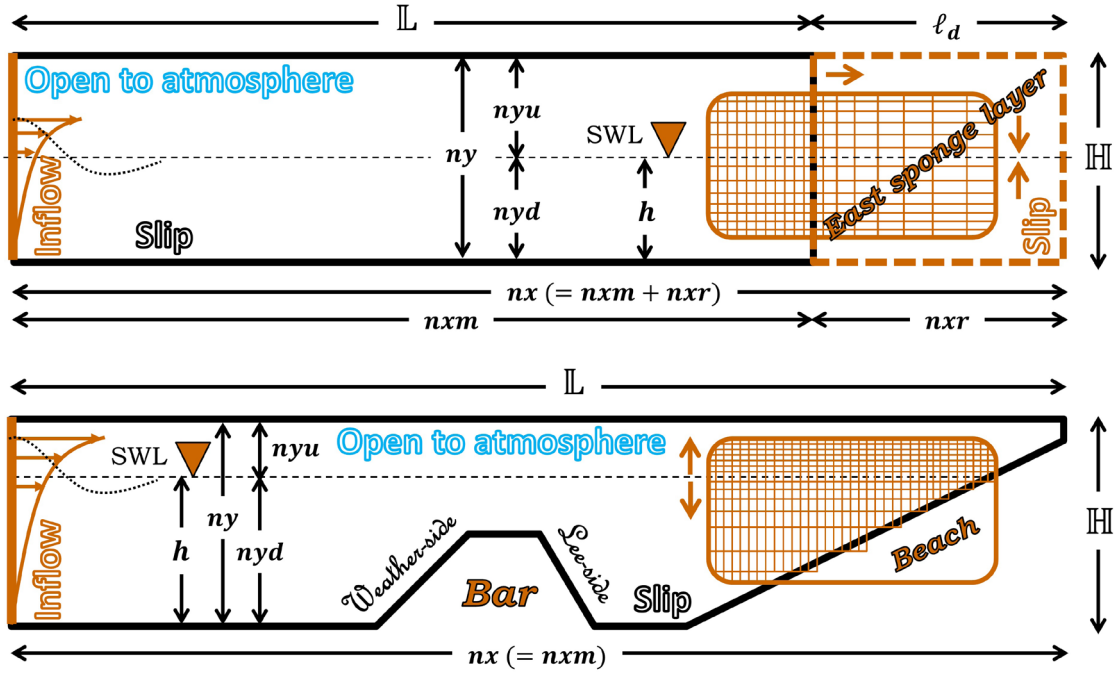

Figure 1: Computational model of the NWT (vertically exaggerated) considered in the present work for *(top)* regular trochoidal wave propagation and *(bottom)* SL wave-structure interaction simulations.

and per wave height ny_H. These variables help in correlating the mesh design to the steepness (H/λ) of the targeted waves. This in turn is helpful in establishing general rules of thumb for selecting optimum mesh refinement for different target wave designs [6].

2.3 Numerical wave generator and sponge-layer design

An inflow boundary-based wavemaker has been employed for wave generation in the present NWT which involves a Dirichlet prescription of $\eta(t)$, $U(y,t)$ and $V(y,t)$ at a vertical boundary (see figure 1). The generator is based on `Stokes V` theory [8] which accurately predicts the dynamics of ocean waves traveling in finite depth and deep water. At fifth order, local free surface displacement $\eta(t)$ is given by,

$$\begin{aligned}\eta(t) =& k^{-1}\left\{A\sin(\omega t) - \left(A^2B_{22} + A^4B_{24}\right)\cos(2\omega t) - \left(A^3B_{33} + A^5B_{35}\right)\sin(3\omega t)\right\} \\ &+ k^{-1}\left\{A^4B_{44}\cos(4\omega t) + A^5B_{55}\sin(5\omega t)\right\} \end{aligned} \tag{4}$$

where, k is circular wavenumber, A is a topological parameter and ω is the circular frequency. The coefficients B_{22}, B_{24} etc. are fractions of polynomials in $\sinh(kh)$ and $\cosh(kh)$ and represent weights assigned to the component harmonics of the `Stokes V` wave [8]. It should be noted that A and k are not known apriori and are inter-related through the equation set (5),

$$A = \frac{0.5kH}{1 + A^2 B_{33} + A^4 \left(B_{35} + B_{55}\right)} \quad \text{and} \quad k = \frac{\left(4\pi^2/gT^2\right)}{\tanh(kh)\left(1 + A^2 C_1 + A^4 C_2\right)} \tag{5}$$

where H is the target wave height, T is wave period and the coefficients C_1 and C_2 govern amplitude dispersion at fifth-order,

$$\begin{aligned} C_1 =& \frac{8c^4 - 8c^2 + 9}{8s^4} \\ C_2 =& \frac{3840c^{12} - 4096c^{10} - 2592c^8 - 1008c^6 + 5944c^4 - 1830c^2 + 147}{512s^{10}\left(6c^2 - 1\right)} \end{aligned}$$

where $s \equiv \sinh(kh)$ and $c \equiv \cosh(kh)$. Equation set (5) is solved iteratively for A and k using initial guesses from linear wave theory. The velocities U, V are in turn derived from the potential $\phi(y,t)$ at fifth order,

$$\begin{aligned} \frac{2\pi T\phi(y,t)}{\lambda^2} =& \left(AA_{11} + A^3A_{13} + A^5A_{15}\right)\cosh(ky)\cos(\omega t) \\ &+ \left(A^2A_{22} + A^4A_{24}\right)\cosh(2ky)\sin(2\omega t) - \left(A^3A_{33} + A^5A_{35}\right)\cosh(3ky)\cos(3\omega t) \\ &- A^4A_{44}\cosh(4ky)\sin(4\omega t) + A^5A_{55}\cosh(5ky)\cos(5\omega t) \end{aligned} \tag{6}$$

where, the coefficients A_{11}, A_{13} etc. are weights assigned to component harmonics of the `Stokes V` wave [8]. Equation (6) represents the "baseline formulation" of the inflow technique [4] which is only suitable for wave generation at low Ursell numbers (Ur). With increasing Ur, there is a non-negligible addition of mass into the domain. Due to a two-phase nature of the simulation, the added mass induces *wave setup* which lessens accuracy. In the present work, the issue of mass addition is addressed through a modified inflow formulation that employs kinematic stretching [9]. Here, the velocity potential ϕ in equation (6) is altered by replacing coordinate y with a stretched coordinate ζ,

$$\begin{aligned} \frac{2\pi T\phi(\zeta,t)}{\lambda^2} =& \left(AA_{11} + A^3A_{13} + A^5A_{15}\right)\cosh(k\zeta)\cos(\omega t) \\ &+ \left(A^2A_{22} + A^4A_{24}\right)\cosh(2k\zeta)\sin(2\omega t) - \left(A^3A_{33} + A^5A_{35}\right)\cosh(3k\zeta)\cos(3\omega t) \\ &- A^4A_{44}\cosh(4k\zeta)\sin(4\omega t) + A^5A_{55}\cosh(5k\zeta)\cos(5\omega t) \end{aligned} \tag{7}$$

such that $\zeta \equiv y \cdot \dfrac{h + \wp}{h + \eta(t)}$ where $\wp > 0$. It is noteworthy that the condition $\wp = 0$ corresponds to Wheeler's method [9] which kinematically over-designs the troughs but under-designs the crests. While Wheeler's method may be suitable for nearly sinusoidal waves at moderate steepness, it significantly under-predicts crest momentum for strongly non-linear waves where the troughs are closer and crests are farther from the SWL. The methodology proposed in equation (7) is novel in that the prescription of $\wp$ is flexible and depends on the wave design in question; the

induced setup can hence be directly controlled using $\wp$. The method described above is termed as the *modified inflow* technique. Trochoidal wave generation using the baseline (equation (6)) and modified (equation (7)) inflow techniques is compared later in section 4.

A wave absorption strategy is essential in NWTs for preventing modulation of the incident wave train by energetic reflections occurring from the far end of the tank. In the present work, incident wave energy has been absorbed/dissipated using a sponge layer for regular wave simulations and a beach for wave-structure interaction simulations. The chief reason for using a beach in the latter case is to closely replicate the experimental conditions of Beji and Battjes [10]. In case of the sponge layer, a combination of momentum damping and grid coarsening [6] has been used for ensuring maximum absorption of incident wave energy. The wave-induced velocity field is damped using equations,

$$\widetilde{U} = \widetilde{U} - \mathbf{e}^{\left(-\alpha(1-x^*)^R\right)}U^n \;\; \text{and} \;\; \widetilde{V} = \widetilde{V} - \mathbf{e}^{\left(-\alpha(1-x^*)^R\right)}V^n \tag{8}$$

where $\widetilde{U}$,$\widetilde{V}$ are predicted values of the streamwise and depthward velocity (neglecting pressure), U^n,V^n are the previous time level values, $\alpha(=10)$ is the strength of the sponge layer, $R(=1)$ controls the variation of damping along the length of the layer and $x^*\left(=\frac{|x-x_a|}{\ell_d}\right)$ is a normalized $x-$coordinate which is zero at the beginning of the sponge layer ($x = x_a$) and unity at the eastern boundary of the tank ($|x - x_a| = \ell_d$). The sponge layer length (ℓ_d) has been selected such that $\ell_d > 3\lambda$. It should be noted that R is kept constant in time and equation (8) is applied *before* correcting the velocity field for continuity. The latter step ensures that the velocity field available for PLIC-VOF advection is divergence-free at the beginning of a new time level. Numerical treatment of submerged structures is described in the next section.

3 Numerical treatment of immersed boundaries

In the present work, immersed boundaries such as bars and beaches have been modeled following an "obstacle approach" (see figure 2). Pressure (or VOF) cell-centers falling inside the outline of the bar/beach are flagged; the flagged cells are skipped during momentum/pressure calculations. The elimination of flagged cells from the domain leads to a characteristic "stair-stepped" approximation to the immersed boundary. It should be noted that no local modifications in cell sizes were introduced for improving said stair-stepped approximations.

The geometrical approximation is followed by local imposition of no-penetration conditions (in U and $V-$momentum) along the entire stair-stepped boundary. A backward-staggered variable arrangement (in addition to maintaining tight pressure-velocity coupling) ensures that U and $V-$momentum cell centers get exactly placed along the stair-stepped approximation thereby greatly simplifying assignment of no-penetration conditions. As observed from figure 2, previously flagged p, f cells are now employed as "ghost cells" (centroid highlighted in yellow) for imposing no-penetration conditions adjacent to fluid cells. It should also be noted that boundary treatment for the beach is identical to that of the bar frontal slope and is not shown here for the sake of brevity.

The proposed methodology thus facilitates a simplified treatment of non-Cartesian geometries in the NWT even when the placement of solution variables is staggered. Wave generation performance of the NWT is evaluated in the next section.

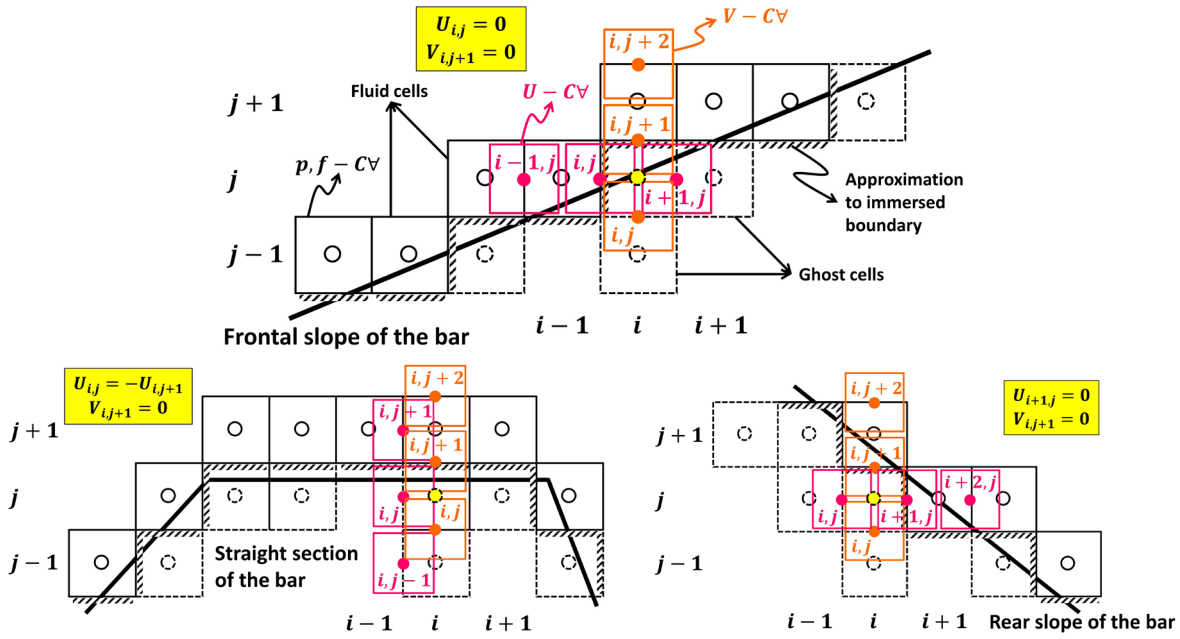

Figure 2: Treatment of immersed boundaries with a "backward staggered" variable arrangement.

4 Results and discussion

The present NWT model is tested for steep (monochromatic) wave generation in near-shallow water as well as propagation and transformation of SL waves over a submerged trapezoidal bar [10]. The first category of problems is used for demonstrating superior volume conservation properties of the proposed inflow boundary. The second category is chosen for testing fidelity of the immersed boundary treatment strategy described in section 3.

4.1 Steep trochoidal waves

Two trochoidal wave designs have been considered; a steep case **C** ($H = 9\,cm, H/\lambda = 0.037, \mathsf{Ur} = 19.5$) [6] and a steeper case $\mathbf{C_a}$ ($H = 12\,cm, H/\lambda = 0.048, \mathsf{Ur} = 27.2$). Both designs are $1.5\,s$ waves propagating in $30\,cm$ deep water ($kh < 0.8$); their topologies being governed by `Stokes V` theory [8]. Identical NWT setups have been considered for both designs. Referring to figure 1, $\mathbb{L} = 19.0\,m$, $\ell_d = 10.0\,m$ and $\mathbb{H} = 0.6\,m$. Corresponding mesh is designed using $nxm = 1330$, $nxr = 50$ (stretched) and $nyu(= nyd) = 25$ (stretched) yielding $nx_\lambda = 170$ and $ny_H = 6$. These values are decided following the design criteria previously established by the authors [6]. Time is non-uniformly advanced with Courant number limited to $C_{max} \leq 0.25$ and time step size limited to $\Delta t_{max} \leq T/750$. Pressure field ($p$) in the simulation is initialized following the hydrostatic law $p = \rho g(h - y)\ \forall\ y \leq h$. The NWT is run for $t = 20T$ in each case.

Results of NWT simulation for cases **C** and $\mathbf{C_a}$ are shown in figure 3. In each case, local variation of free surface elevation measured $+6\lambda$ away from the wavemaker is compared for baseline ($\wp = \eta(t); \zeta \equiv y$) and modified ($\wp > 0\ \forall\ y < h; \wp = \eta(t)\ \forall\ y \geq h$) inflow formulations. A superior performance of the proposed "modified inflow" boundary is clearly evident as setup

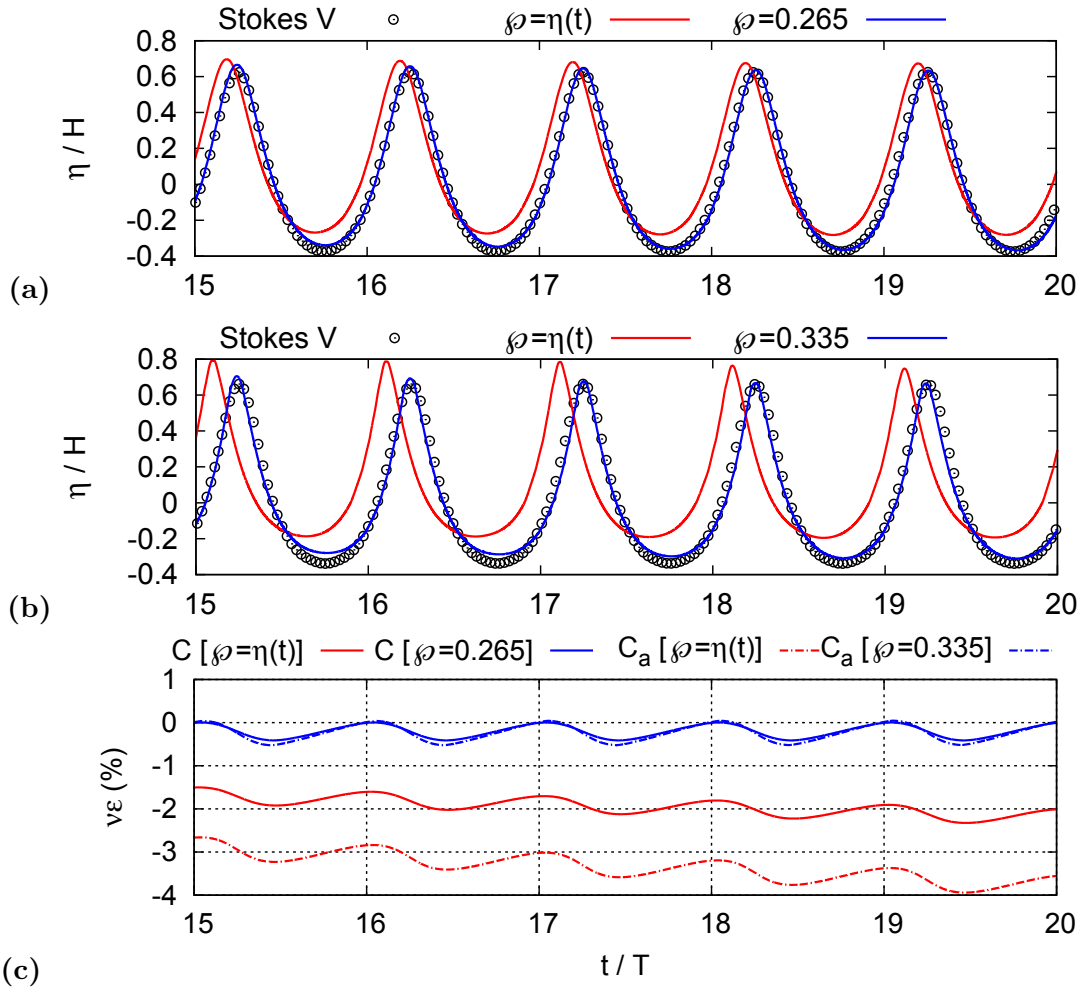

Figure 3: Trochoidal wave generation performance of the proposed NSE-based NWT model illustrated using $\eta(t)$ signals measured $+6\lambda$ from the wavemaker for cases (a) $\mathbf{C}$ and (b) $\mathbf{C_a}$ and (c) time variation of volume error ($\mathcal{VE}$) during last five wave periods of the simulation.

induced in wave topology due to volume addition is convincingly nullified (figures 3 (a,b)). The baseline and modified inflow configurations are also compared based on percentage change in primary phase (water) volume ($\mathcal{VE}$) within the NWT [6] during last five wave periods (figure 3 (c)). It is seen that there is net volume addition over a wave period in the baseline formulation ($\wp = \eta(t)$) whose magnitude increases with steepness H/λ. This is also evident from the stronger setup induced for case $\mathbf{C_a}$ in figure 3 (b). It naturally follows that the "optimum" value of $\wp$ required for exactly balancing volume addition would also increase with H/λ which is indeed the case from figure 3. It should be noted that $\wp = 0.265$ and $\wp = 0.335$ considered for cases $\mathbf{C}$ and $\mathbf{C_a}$ (respectively) have been determined parametrically (said analysis not shown here).

Results demonstrate that the proposed modified inflow boundary based NWT is volume preserving and that momentum over-design imposed below the SWL does not induce any wave

distortion far from the wavemaker. Wave-structure interaction simulations performed using (only) the modified inflow formulation are presented next.

4.2 Wave transformation over a submerged trapezoidal bar

Long wave propagation over barred topographies is characterized by extensive short wave generation on the lee side [10] which offers an invaluable strategy for coastal protection. Simulation of wave transformation scenarios poses a unique difficulty in terms of optimizing spatio-temporal resolution in the NWT because H/λ and kh are *variable* along the direction of propagation.

In the present work, it is aimed to replicate SL wave transformation experiments of Beji and Battjes [10]. The experiments involve propagation of small steepness ($H = 2\,cm, H/\lambda = 0.005$), low frequency ($T = 2.0\,s$) waves in $40\,cm$ deep water ($kh = 0.68$) over a submerged bar and the "transformed" wave train is eventually dissipated over a gently sloping beach; geometries

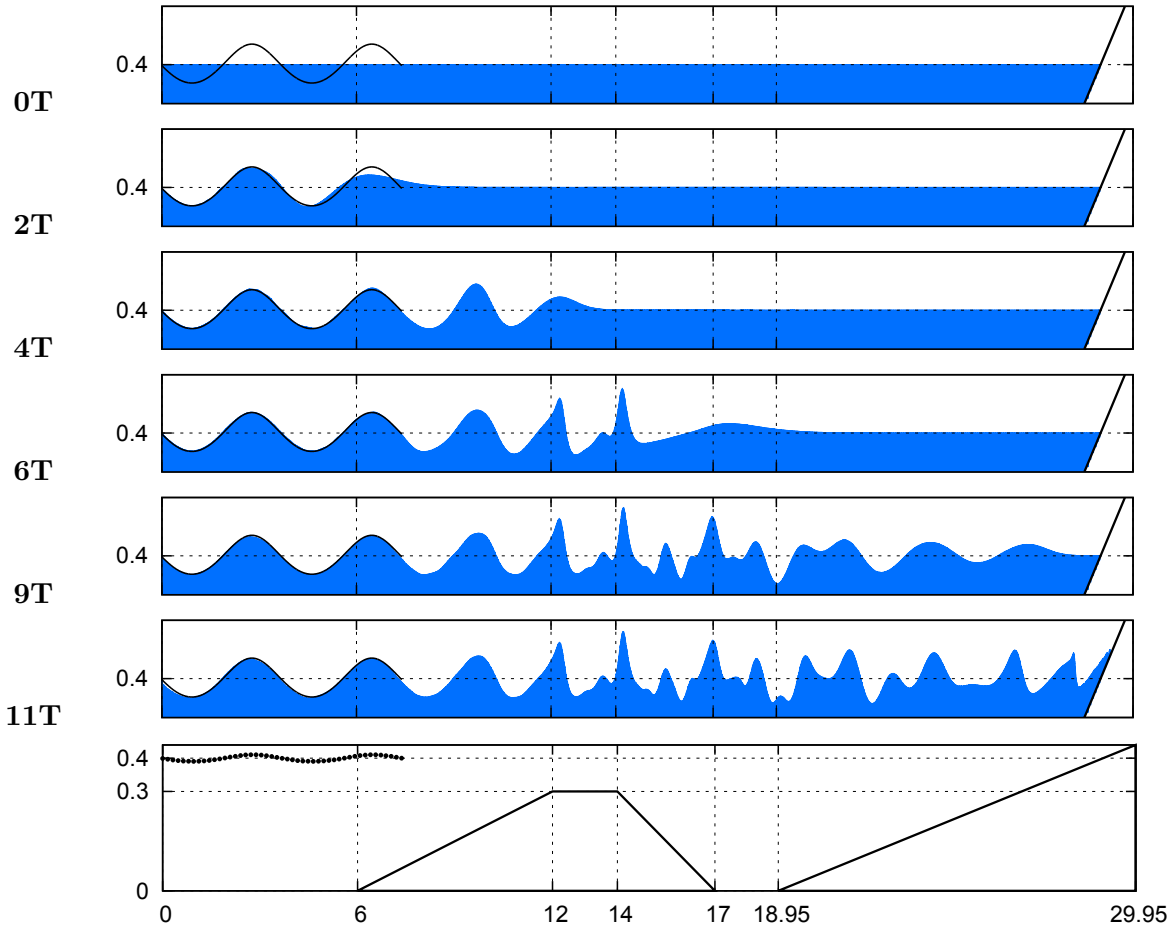

Figure 4: Time series of spatial profiles $\eta(x)$ showing non-breaking transformation of sinusoidal low frequency waves ($H = 0.02\,m, T = 2\,s, h = 0.4\,m$) propagating over a submerged trapezoidal bar for a duration of $t = 11T$. Geometries of the bar and beach are shown at the bottom; coordinates are in m.

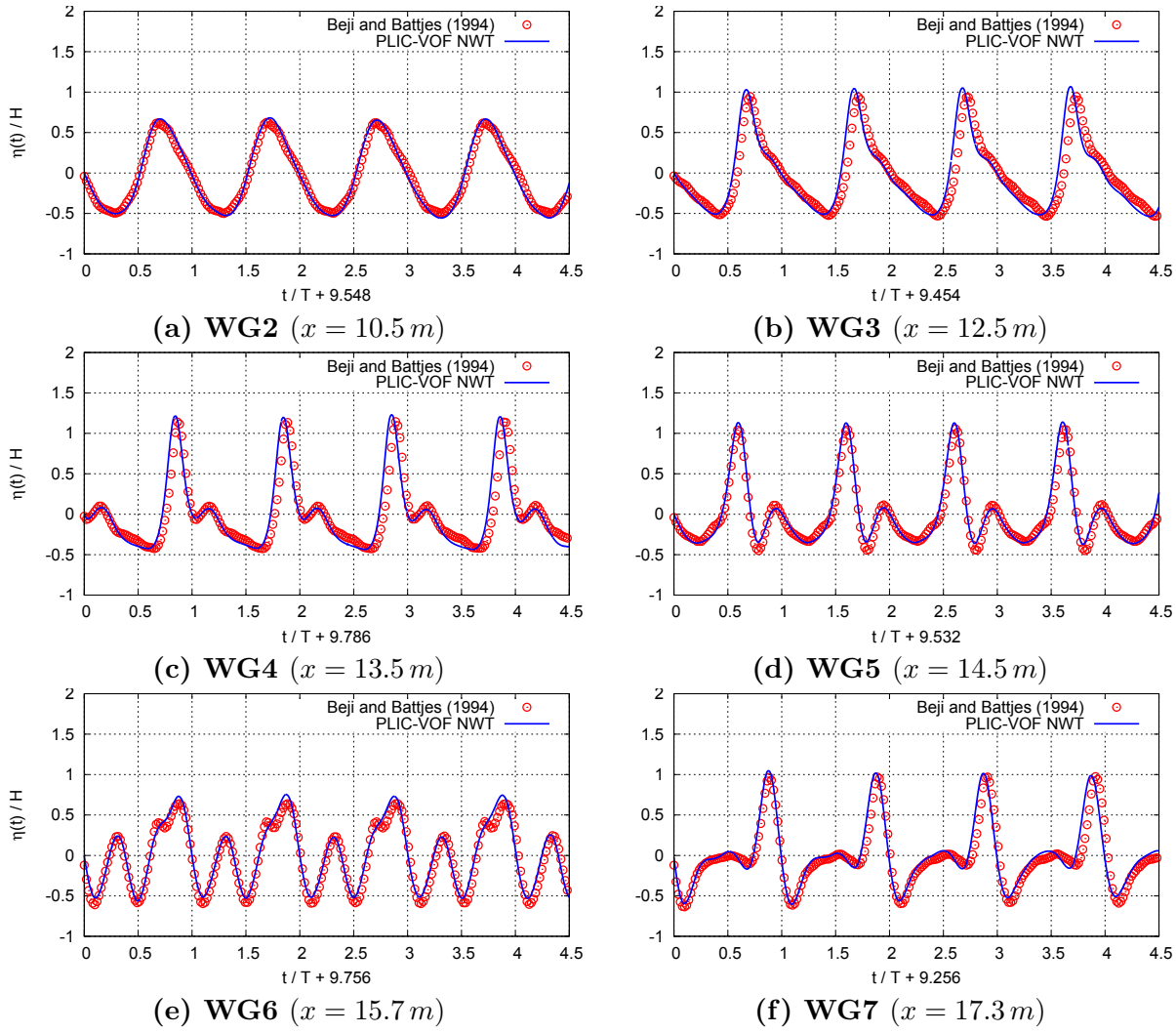

(a) WG2 ($x = 10.5\,m$) **(b) WG3** ($x = 12.5\,m$)

(c) WG4 ($x = 13.5\,m$) **(d) WG5** ($x = 14.5\,m$)

(e) WG6 ($x = 15.7\,m$) **(f) WG7** ($x = 17.3\,m$)

Figure 5: Validation of normalized free surface elevation signals measured at six wave gauge locations (**WG2**–**WG7**) [10] in the NWT after a passage of nine wave periods for a duration of $t = 4.5T$.

of the bar and beach are shown, to scale, in figure 4. Despite the fact that $H/\lambda = 0.005$, $\mathsf{Ur} = 4.27$ which renders the waves slightly trochoidal thereby necessitating `Stokes V` theory for representation. Correlating Beji and Battjes' setup to the computational model in figure 1, $\mathbb{L} = 29.95\,m$, $\mathbb{H} = 0.44\,m$ and $h = 0.4\,m$. Mesh design is characterized by $nxm(= nx) = 1500$, $nyu = 20$ and $nyd = 26$ (stretched) yielding $nx_\lambda = 185$ and $ny_H = 10$. Given small steepness of the upstream waves, Δt_{max} was (conservatively) set to $T/5000$ (following parametric investigations not shown here) with $C_{max} \leq 0.25$; the limiting value C_{max} was only exceeded during initial breaking at the beach. Pressure field within "fluid cells" (see figure 2) was initialized using the hydrostatic law and the simulation was run for $t = 15T$.

Major stages of the wave transformation process are highlighted in figure 4. The SL waves

initially shoal over the front (seaward) face of the bar and become progressively asymmetrical ($t = 4T$). Triplet resonance occurs over the straight portion of the bar [10] which generates dispersive trailing "free" waves ($t = 6T$). As the train "de-shoals" [10] behind the bar, the primary wave breaks up into several smaller amplitude waves with nearly harmonic frequencies ($t > 9T$). The present simulations have also been compared against local free surface elevation $\eta(t)$ measurements of Beji and Battjes at six wave gauge locations (see figure 5). The comparison is initiated from a downcrossing in each case and, barring minor phase differences at some stations, the overall agreement between PLIC-VOF NWT and experiments is good. The phase difference is (probably) attributable to a forward Euler method being used for time advancement; it is aimed to increase the order of time discretization in the near-future.

5 Conclusion

We propose a volume preserving, wave-inflow technique and a simplified numerical treatment of immersed boundaries for NSE-based NWTs. Said methods have been successfully benchmarked against steep wave generation and wave-structure interaction scenarios for $kh < 0.8$.

REFERENCES

[1] Kamath, A., Bihs, H. and Arntsen, Ø.A. Numerical investigations of the hydrodynamics of an oscillating water column device. *Ocean Eng.* (2015) **102**:40–50.

[2] Sriram, V., Sannasiraj, S.A. and Sundar, V. Simulation of 2-D nonlinear waves using finite element method with cubic spline approximation. *J. Fluid Struct.* (2006) **22**:663–681.

[3] Boccotti, P. *Wave Mechanics for Ocean Engineering.* Elsevier Science B.V., Elsevier Oceanography Series Vol. 64, (2000).

[4] Lin, P. and Liu, P.L-F. A numerical study of breaking waves in the surf zone. *J. Fluid Mech.* **359**:239–264.

[5] Lin, P. and Liu, P.L-F. Internal Wave-Maker for Navier-Stokes Equations Models. *J. Waterw. Port C-ASCE* (1999) **125**:207–215.

[6] Saincher, S. and Banerjee, J. On wave damping occurring during source-based generation of steep waves in deep and near-shallow water. Revision submitted to *Ocean Eng.* (2016).

[7] Perić, R. and Abdel-Maksoud, M. Generation of free-surface waves by localized source terms in the continuity equation. *Ocean Eng.* (2015) **109**:567–579.

[8] Fenton, J.D. A fifth-order Stokes theory for steady waves. *J. Waterw. Port C-ASCE* (1985) **111**:216–234.

[9] Wheeler, J.D. Method for calculating forces produced by irregular waves. *J. Petrol. Technol.* (1970) **22**:359–367.

[10] Beji, S. and Battjes, J.A. Numerical simulation of nonlinear wave propagation over a bar. *Coast. Eng.* (1994) **23**:1–16.